

Hybrid coherent control of magnons in a ferromagnetic phononic resonator excited by laser pulses

Alexey V. Scherbakov^{1,*}, Alex D. Carr², Tetiana L. Linnik^{1,3}, Serhii M. Kukhtaruk³, Andrew D. Armour², Achim Nadzeyka⁴, Andrew W. Rushforth², Andrey V. Akimov², and Manfred Bayer¹

¹*Experimentelle Physik 2, Technische Universität Dortmund, 44227 Dortmund, Germany*

²*School of Physics and Astronomy, University of Nottingham, Nottingham NG7 2RD, United Kingdom*

³*Department of Theoretical Physics, V. E. Lashkaryov Institute of Semiconductor Physics, 03028 Kyiv, Ukraine*

⁴*Raith GmbH, 44263 Dortmund, Germany*



(Received 3 July 2023; revised 15 November 2023; accepted 22 November 2023; published 23 January 2024)

We propose and demonstrate the concept of hybrid coherent control (CC) whereby a quantum or classical harmonic oscillator is excited by two excitations: one is quasiharmonic (i.e., harmonic with a finite lifetime) and the other is a pulsed broadband excitation. Depending on the phase relation between the two excitations, controlled by the detuning of the oscillator eigenfrequencies and the wave forms of the quasiharmonic and broadband excitations, it is possible to observe Fano-like spectra of the harmonic oscillator due to the interference of the two responses to the simultaneously acting excitations. Experimentally, as an example, the hybrid CC is implemented for magnons in a ferromagnetic grating where GHz coherent phonons act as the quasiharmonic excitation and the broadband impact arises from pulsed optical excitation followed by spin dynamics in the ferromagnetic nanostructure.

DOI: [10.1103/PhysRevResearch.6.L012019](https://doi.org/10.1103/PhysRevResearch.6.L012019)

Coherent control (CC) is well established as a powerful method to manipulate the amplitude and phase of quantum states. First used for chemical reactions [1,2], CC has been demonstrated for single electrons [3], spins [4,5], nanoelectromechanical oscillators [6], magnons [7,8], and other systems [9]. The basic phenomenon governing CC is the interference of the responses of a quantum system to specific excitations, which determine the phase of the wave function. One of the common technical solutions for realizing CC is to use two optical pulses from ultrafast lasers with adjustable time separation or more sophisticated laser pulse shaping [10]. For CC of magnons, two microwave pulses may be used [11]. Traditionally, the excitations that lead to the interfering responses have the same origin, e.g., transitions between the ground and an excited quantum state are induced by a resonant electromagnetic field. However, there are quantum systems that may be excited by a pair of excitations of different origins. For example, one excitation may be broadband and the other harmonic. Exploiting a combination of various types of excitations for *hybrid* CC would broaden a diversity of CC applications for quantum computing and communications.

The idea of hybrid CC in the spectral domain is illustrated in Figs. 1(a) and 1(b) for a linear tunable quantum or classical oscillator with eigenfrequency ω_0 and finite lifetime. Figures 1(a) and 1(b) show the amplitude spectra of the

oscillator's responses to two types of excitation: (1) quasiharmonic (i.e., harmonic with finite lifetime) excitation with central frequency ω_R detuned relative to ω_0 , and (2) broadband excitation. Two cases of detuning are considered: negative ($\omega_0 < \omega_R$) in Fig. 1(a) and positive ($\omega_0 > \omega_R$) in Fig. 1(b). The top blue curves show the spectra when only quasiharmonic excitation is present. In this case the phase ϕ of the oscillator at $\omega = \omega_0$ changes by π when the oscillator eigenfrequency is tuned through the resonance $\omega = \omega_R$, say from $-\pi/2$ to $\pi/2$ as demonstrated in the comparison of the blue spectra in Figs. 1(a) and 1(b). The middle red curves are spectral responses when the oscillator is excited by a broadband excitation (2). The oscillator's phase ϕ , e.g., $\phi = \pi/2$, at $\omega = \omega_0$ in this case does not depend on ω_0 . The lower black curves are the spectra when the two excitations, (1) and (2), operate together. Clearly, we get destructive [Fig. 1(a)] or constructive [Fig. 1(b)] interference of the oscillator's responses at $\omega = \omega_0$ depending on the detuning of the oscillator eigenfrequency relative to the central frequency of the quasiharmonic excitation, $\omega_0 < \omega_R$ or $\omega_0 > \omega_R$, respectively. For negative detuning ($\omega_0 < \omega_R$) the response is almost zero, while at positive detuning ($\omega_0 > \omega_R$) the spectral amplitude at $\omega = \omega_0$ increases by a factor of two. The interference effects represent an example of hybrid CC where two excitations have different spectra and are of different nature; for example (1) could be a coherent phonon wave packet and (2) could be a short microwave or laser pulse. By varying the detuning, amplitudes, and phases of excitations (1) and (2), it is possible to model various Fano-like spectral shapes similar to Fano spectra which appear as a result of interference of broad- and narrow-band eigenstates [12].

In the present Letter we demonstrate an example where CC is realized for the case of magnons. Magnons are a typical example for which a diversity of quantum excitations

*alexey.shcherbakov@tu-dortmund.de

Published by the American Physical Society under the terms of the [Creative Commons Attribution 4.0 International](https://creativecommons.org/licenses/by/4.0/) license. Further distribution of this work must maintain attribution to the author(s) and the published article's title, journal citation, and DOI.

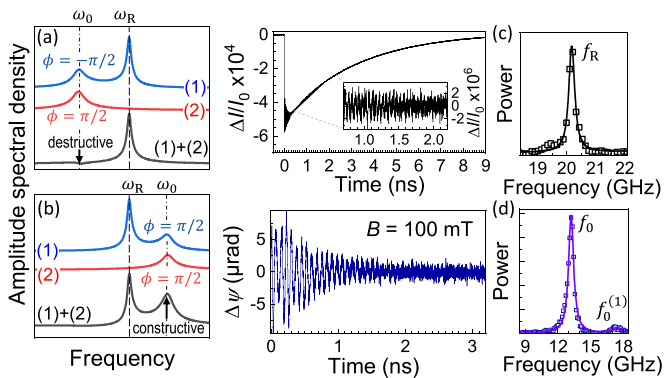


FIG. 1. (a), (b) Concept of hybrid coherent control. Model spectra of an oscillator with eigenfrequency ω_0 excited by quasiharmonic (1) and broadband (2) excitations with negative (a) and positive (b) detuning; upper, middle, and lower spectra correspond to separate excitations (1), (2), and the result of joint excitation, respectively. (c), (d) Temporal signals (left, background subtracted in the inset) and their FFT (right) for the probe intensity (c) and polarization rotation angle (d).

exists [13]. The quasiharmonic excitation of magnons is coming from quasi-monochromatic surface phonons. They drive the spectrally isolated magnon mode at the frequency ω_R . The broadband excitation is based on ultrafast modulation of the ferromagnet magnetization. Both excitations are triggered optically by a femtosecond laser pulse. The magnon eigenfrequency ω_0 is tuned by the external magnetic field \mathbf{B} . Monitoring the magnon spectrum, we observe destructive or constructive interference in the responses to the joint excitations, depending on the magnon-phonon detuning and relative phases of the excitations.

The sample studied consists of a 20-nm-thick ferromagnetic metallic layer (we chose the $\text{Fe}_{0.81}\text{Ga}_{0.19}$ alloy known as galfenol [14]) grown on a GaAs (001) substrate. The surface of the ferromagnetic layer is patterned in the form of a one-dimensional lateral nanograting (NG) with a period $d = 120$ nm. The parallel grooves of 7-nm depth and 48-nm width are milled by focused Ga^+ ion beam parallel to the [010] crystallographic direction. The periodic spatial profile and modulated magnetic properties [15–17] determine the spectra and spatial profiles of the phonon and magnon modes [18–20] (see Supplemental Material [21] for the details).

The ferromagnetic layer is excited from the substrate side by pump pulses from a Yb-doped fiber-based laser oscillator (1050-nm wavelength, 80-MHz repetition rate, 150-fs pulse duration) with maximum fluence $J_0 \sim 10$ mJ/cm² in a spot of 3- μm diameter. The pump pulse excites coherent phonons and magnons in the ferromagnet [22,23]. To monitor the coherent phonons and magnons in the time domain we measure the intensity changes $\Delta I(t)$ and the polarization rotation $\Delta\psi(t)$ of the linearly polarized probe pulses (780-nm wavelength, 150-fs pulse duration, 1- μm spot size) reflected from the NG surface [22,24]. We use asynchronous optical sampling (ASOPS [25]) to measure the transient signals with 1-ps time resolution in a 12.5-ns time window (see Supplemental Material [21] for the details). The sample is mounted at ambient temperature in a magnetic field \mathbf{B} applied in the

plane of the ferromagnetic layer at 45 degrees to the direction of the grooves.

Figures 1(c) and 1(d) show the signals $\Delta I(t)$ and $\Delta\psi(t)$, respectively, and their power spectra. The intensity signal $\Delta I(t)$ in Fig. 1(c) oscillates on a slowly decaying thermal background. The oscillations are characterized by two frequencies: 45 GHz and 20.1 GHz. The fast-decaying 45-GHz oscillations are due to Brillouin oscillations of the probe pulse reflection at the phonon wave packet injected into the GaAs substrate [26]. The oscillations at 20.1 GHz correspond to the generalized Rayleigh wave in the NG [18]. Its spectral line in the fast Fourier transform (FFT) of the transient signal has a width of 0.2 GHz, which corresponds to a Q factor $Q \sim 100$. The transient polarization rotation signal $\Delta\psi(t)$, shown in Fig. 1(d) for $B = 100$ mT (far from the magnon-phonon resonance), is dominated by the lowest magnon mode corresponding to the quasiniform spin precession with eigenfrequency $f_0 = 13.2$ GHz. A second magnon mode with eigenfrequency $f_0^{(1)} = 17.4$ GHz is also detected in the magnon spectrum [see the right panel in Fig. 1(d)]. In the used range of external magnetic field the magnon eigenfrequencies depend linearly on B , and the resonance of the lowest magnon mode and the Rayleigh phonon mode ($f_0 = f_R$) is observed at $B_{\text{res}} = 280$ mT.

The studied system has similarities with the model linear oscillator presented in Figs. 1(a) and 1(b) to demonstrate the idea of hybrid CC. Indeed, the magnons with eigenfrequency $f_0 = \omega_0/2\pi$ are the analog of the linear quantum oscillator the eigenfrequency of which is controlled by the external magnetic field. The Rayleigh phonons with frequency $f_R = \omega_R/2\pi$ are the analog of the quasiharmonic excitation (1) which drives magnons at f_R [27]. The laser pulse triggers spin precession taking the role of the broadband excitation for magnons (2).

The contribution of the quasiharmonic phonon driving at the frequency $f_R = 20.1$ GHz leading to the expected interference effects becomes noticeable at a smaller detuning ($f_R \sim f_0$), which is achievable by the external magnetic field B . Figure 2 presents the results for the B dependencies of the measured magnon spectra at two pump fluences J . Figures 2(a) and 2(b) show the spectra measured at maximum fluence $J = J_0$. It is seen that in the chosen range of B , the magnon spectrum consists of three spectral lines: the line at $f \approx f_R$, and two lines centered at the field-dependent magnon eigenfrequencies f_0 and $f_0^{(1)}$. The spectral amplitude at $f \approx f_R$ has a maximum at $B = 270$ mT, close to the magnon-phonon resonance, $f_0 = f_R$, that happens at $B_{\text{res}} = 280$ mT. The magnon spectra in the vicinity of the magnon-phonon resonance are strongly asymmetric, similar to Fano resonance spectra [12]. The typical feature of the obtained spectrum is a dip at the low-frequency side relative to the magnon-phonon resonance. This dip is found in the spectra in the range of B marked by the dashed circle in Fig. 2(b). Another interesting feature is a higher magnon spectral amplitude at $B > B_{\text{res}}$ relative to that at $B < B_{\text{res}}$. This feature, together with the aforementioned nulling of the magnon amplitude, is clearly demonstrated in Fig. 2(c), where the amplitude A_0 at the magnon eigenfrequency $f = f_0$ is plotted vs B . The nulling of the magnon amplitude takes place at detuning $f_R - f_0 = 0.4$ GHz and the corresponding magnon spectrum

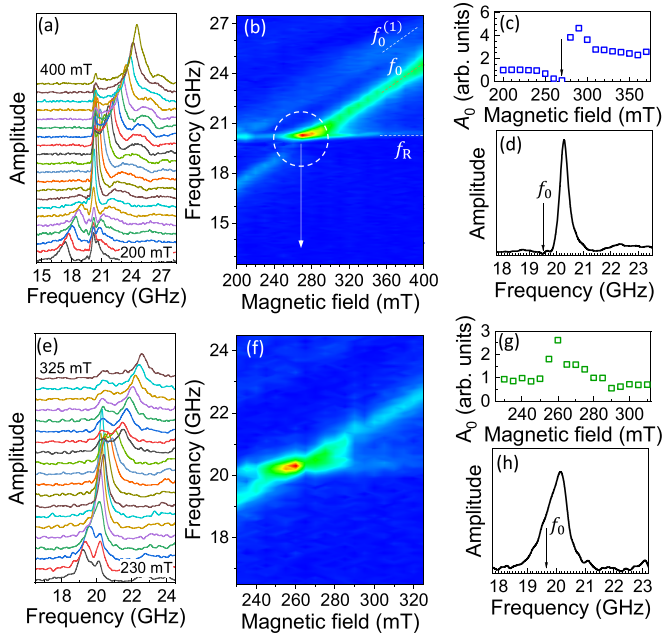


FIG. 2. The measured spectra of magnons. [(a)–(d)] High pump fluence $J = J_0$. (e)–(h) Low pump fluence $J = 0.1J_0$. [(a), (e)] Magnon spectra for various B . (b), (f) The spectra as color maps; the dashed circle in (b) marks the area around the magnon-phonon resonance and the vertical arrow points at the B corresponding to destructive interference. (c), (g) The dependencies of the amplitude A_0 at the magnon eigenfrequency f_0 on B ; the vertical arrow in (c) points at the field where the nulling of A_0 takes place. (d), (h) The magnon spectra for the same detuning $f_R - f_0 = 0.4$ GHz, which corresponds to $B = 270$ mT (d) and 250 mT (h), respectively.

shown in Fig. 2(d) has only one spectral line with a maximum at $f = 20.3$ GHz, which is 0.2 GHz higher than the frequency of phonon excitation.

The Fano-like spectra are not observed for low fluence $J \sim 0.1J_0$ for which the spectra and a color map are presented in Figs. 2(e) and 2(f). There is no nulling of A_0 at any B and the amplitude A_0 is higher at $B < B_{\text{res}}$ than at $B > B_{\text{res}}$ [see Fig. 2(g)], contrary to what is obtained at high J . The magnon spectrum at the detuning $f_R - f_0 = 0.4$ GHz shown in Fig. 2(h) possesses an asymmetry that has completely different features from the case of high J [compare with the spectrum in Fig. 2(d)].

The results presented in Fig. 2 for high J [panels (a)–(d)] show qualitative agreement with the concept of hybrid CC demonstrated in Figs. 1(a) and 1(b). Indeed, magnons excited by two different kinds of excitation show destructive interference resulting in nulling of the magnon amplitude at a certain value of negative detuning. Constructive interference results in an increase of the magnon amplitude for positive detuning. The interference effects at low J [panels (e)–(h) in Fig. 2] are not as pronounced as at high J , which points to a dependence of the phase and amplitude relations of the two excitations on the pump fluence.

To understand the physics of hybrid CC for magnons we have to consider the magnon wave function as a quantum oscillator excited by two types of excitations. It is possible to show [21,28–30] that this task may be converted to the

consideration of a classical oscillator and, thus, to the solution of the Landau-Lifshitz-Gilbert equation [13] for the normalized magnetization, \mathbf{m} , precessing in the time-dependent effective field, $\mathbf{B}_{\text{eff}}(t)$, altered by ultrashort optical excitation and driven by coherent phonons. The phonon driving is modeled as a small perturbation in $\mathbf{B}_{\text{eff}}(t)$ through the ac field $\delta\mathbf{B}_R(t)$: $\mathbf{B}_{\text{eff}}(t) = \mathbf{B}_0 + \delta\mathbf{B}_R(t)$, where \mathbf{B}_0 is a stationary component of the effective field. Due to the in-plane orientation of \mathbf{B}_0 , for a Rayleigh wave with the wave vector along the x axis (perpendicular to the grooves) only the longitudinal strain component ε_{xx} contributes to $\delta\mathbf{B}_R(t)$ [21,31]. Thus, only the x projection of $\delta\mathbf{B}_R(t)$ is nonzero: $\delta B_{Rx}(t) = -2b_1\varepsilon_{xx}(t)m_{0x}$, where b_1 is the magnetoelastic coefficient and m_{0x} is the x projection of the stationary normalized magnetization. The dynamical strain $\varepsilon_{xx}(t)$ excited by the pump pulse at $t = 0$ is

$$\varepsilon_{xx}(t) = -\varepsilon_0 \sin(\omega_R t) \exp(-\Gamma_R t/2), \quad (1)$$

where ε_0 , $\omega_R = 2\pi f_R$, and Γ_R are the strain amplitude, the phonon eigenfrequency, and the decay rate, respectively.

The broadband excitation of magnons is a result of the ultrafast electron and lattice heating of the ferromagnet induced by the laser pulse. It leads to the decrease of the saturation magnetization M_0 affecting the demagnetizing fields [23]. Because the heating is nonuniform with temperature gradients between the grooves and ridges of the NG [21], it results also in a sub-picosecond pulse of diffusive current of spin-polarized electrons [32–38]. Both contributions can be modeled [39] by a time-dependent field, $\delta\mathbf{B}_m(t)$, the temporal profile of which governs the phase relations between the broadband and quasiharmonic excitations.

Assuming small precession amplitudes, the LLG equation can be modified to a linear second-order differential equation for the deviation of the azimuthal angle, $\delta\varphi(t)$, of \mathbf{m} from equilibrium [40]. This equation is identical to the equation of a linear oscillator with quasiharmonic excitation as an external force while the ultrafast broadband excitation is included in the initial conditions. The solution of this linear equation may be written as

$$\delta\varphi(t) = \delta\varphi_{\text{ph}}(t) + [\delta\varphi(0) \cos(\omega_0 t) + \delta\dot{\varphi}(0)\omega_0^{-1} \sin(\omega_0 t)] \exp(-\Gamma_0 t/2), \quad (2)$$

where Γ_0 is the magnon damping rate. The first term in Eq. (2) is a partial solution from the modulation by phonons (see Supplemental Material [21]) and the expression in the square brackets is the general solution with the initial conditions at $t = 0$ for displacement $\delta\varphi(0)$ and velocity $\delta\dot{\varphi}(0)$ determined by the broadband excitation. The resulting $\delta\varphi(t)$ is the interference of the partial and general solutions, in which the phases of $\delta\varphi(0)$ and $\delta\dot{\varphi}(0)$ at $\omega = \omega_0$ determine the interference between the quasiharmonic and broadband excitations. The values $\delta\varphi(0)$ and $\delta\dot{\varphi}(0)$ are governed by the time evolution of $\delta\mathbf{B}_m(t)$. Let us consider two extreme cases: (i) *Displacive excitation* when $\delta\mathbf{B}_m(t)$ has the form of an instantaneous step. In this case the initial speed $\delta\dot{\varphi}(0) = 0$. (ii) *Impulsive excitation* when the broadband excitation is applied in the form of an ultrashort pulse. Then the initial displacement $\delta\varphi(0) = 0$. The phase relations between

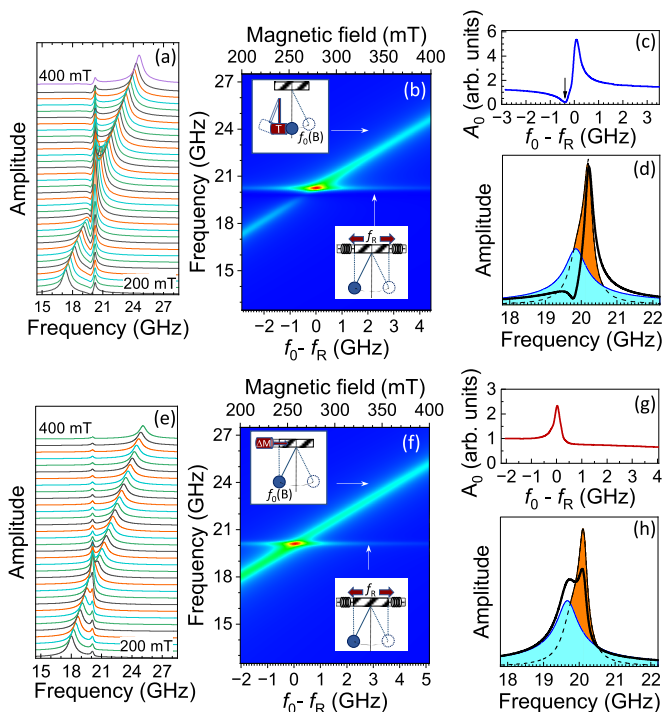


FIG. 3. The simulated spectra of magnons. (a)–(d) The spectra calculated for the case of broadband impulsive excitation. [(e)–(h)] The spectra calculated for the case of broadband displacive excitation. [(a), (e)] Magnon spectra for various B . (b), (f) The spectra as color maps; the insets demonstrate the analogy with a pendulum excited by the impact of a load (b) or displacement (f) in parallel with a quasiharmonic force with central frequency f_R (lower inset). (c), (g) The dependencies of the spectral amplitude A_0 at the magnon eigenfrequency f_0 on B ; vertical arrow in (c) points at the B where nulling of A_0 takes place due to destructive interference. (d), (h) The magnon spectrum (thick black line) calculated for the detuning $f_R - f_0 = 0.4$ GHz when the phonon driving and the broadband laser pulse excite magnons in parallel; thin lines are the magnon spectra when excited separately by phonon driving (red shading) or broadband pulse (blue shading).

broadband and phonon excitations at the frequency of the magnon resonance ω_0 differ by $\pi/2$ depending on whether the excitation is displacive or impulsive. It is easy to show from Eq. (2) that for our damping rates Γ_0 and Γ_R , the interference will be destructive or constructive depending on the detuning of the magnon and phonon resonances when the broadband excitation is impulsive. For displacive broadband excitation the partial and general solutions in Eq. (2) are close to orthogonal and interference does not take place. Such a simplified consideration based on Eq. (2) clearly shows how the hybrid CC works for magnons.

The results of the modeling for impulsive and displacive excitation are summarized in Fig. 3 (see Supplemental Material for the full set of parameters). Comparing the simulation for impulsive excitations [Figs. 3(a)–3(d)] and the experimental results for high J [Figs. 2(a)–2(d)] we find the following agreement: the nulling of A_0 takes place when the eigenfrequency is shifted from the phonon frequency by 0.4 GHz pointing to destructive interference; A_0 has a higher value at $f_0 > f_R$ in comparison to $f_0 < f_R$. The experimental results

for low J [Figs. 2(e)–2(h)] agree well for the theory which exploits displacive excitation [Figs. 3(e)–3(h)]. There the spectra do not show distinct Fano features such as nulling. Such dependence on excitation fluence leads us to conclude that the phase relations between the broadband and quasiharmonic excitations of magnons are different for high and low pump fluences.

The physics of the displacive and impulsive broadband excitations and their dependencies on J is based on the ultrafast spin dynamics in the studied structure. At low J , optical excitation induces ultrafast demagnetization with slow recovery, and $\delta\mathbf{B}_m(t)$ is well described by the step function (displacive excitation) [23,41]. Increasing J results in a strong magnetic nonuniformity due to the lower Curie temperature in the grooves. In this case the diffusive spin current between the grooves and ridges leads to a torque on \mathbf{m} which increases with increasing J . The spin current and corresponding torque pulse last less than 1 ps due to rapid electron thermalization, so that $\delta\mathbf{B}_m(t)$ may be considered as a temporal delta function (impulsive excitation) [32–38]. The dependence of the magnon spectra on the pump fluence shows the gradual transformation of the broadband excitation from displacive to impulsive with the increase of J (for details, see Supplemental Material [21]).

The studied structure is an example of systems where the hybrid CC can be realized. The requirements for efficient CC include narrowband spectral profiles for both the driven oscillator and the driving quasiharmonic excitation and controllable detuning of their eigenfrequencies, and relative phases. In the considered case of a ferromagnetic nanostructure, the long lifetime of the magnon mode is provided by the ferromagnet's properties [42] and the small thickness of the ferromagnetic layer, which results in the mode's spectral isolation [43]. Periodic spatial patterning is responsible for the high- Q factor of the Rayleigh phonon mode and allows tuning the initial phase of the broadband optical excitation by the fluence-dependent excitation mechanism: ultrafast demagnetization or spin diffusion. The combination of these features was not met in earlier works on the optically triggered phonon driving of magnetization [44–50].

There are other systems, which are characterized by high- Q resonances and can be excited by broadband and harmonic excitations, and, thus, are suitable for hybrid CC. Examples are multiple photonic cavities [51] or a single photonic cavity coupled to a mechanical oscillator [52], single spins [53,54] and spin ensembles [55], magnon-phonon and magnon-photon hybrid systems [56–58], spin-valve ferromagnetic structures [35], magnons in antiferromagnets [59,60], hydrogen molecules [61], and many others.

In conclusion, we present the concept of hybrid coherent control where a linear quantum or classical oscillator is excited by two different types of excitations: broadband and quasiharmonic. We confirm the feasibility of this concept experimentally by exploiting magnons in a patterned ferromagnetic film excited by a femtosecond laser pulse, which triggers an ultrafast demagnetization and generates coherent phonons. The concept of hybrid coherent control fits well in the wide field of Fano resonances that are prospective for various applications in quantum technologies [62]. For instance, the nulling effect of the amplitude at the oscillator

resonance frequency observed in our work has similarity with electromagnetic induced transparency [63] but happens without modification of the permittivity by nonlinear or special coupling effects.

We are grateful to Anton Samusev, Ilya Akimov, and Vladimir Korenev for fruitful discussions. The work was supported by Deutsche Forschungsgemeinschaft through the project SFB TRR160 (project A1), the research center

“Future Energy Materials and Systems” of the Research Alliance Ruhr, and the Engineering and Physical Sciences Research Council (Grant No. EP/V056557/1). The cooperation between TU Dortmund and the Lashkaryov Institute was supported by the Volkswagen Foundation (Grant No. 97758). A.V.A. acknowledges the Alexander von Humboldt Foundation. T.L.L. acknowledges the Alexander von Humboldt Foundation support through the Philipp Schwartz initiative and TU Dortmund core funds.

-
- [1] W. S. Warren, H. Rabitz, and M. Dahleh, Coherent control of quantum dynamics: The dream is alive, *Science* **259**, 1581 (1993).
- [2] L. Zhu, V. Kleiman, X. Li, S. P. Lu, K. Trentelman, and R. J. Gordon, Coherent laser control of the product distribution obtained in the photoexcitation of HI, *Science* **270**, 77 (1995).
- [3] C. Bäuerle, D. C. Glatzli, T. Meunier, F. Portier, P. Roche, P. Roulleau, S. Takada, and X. Waintal, Coherent control of single electrons: A review of current progress, *Rep. Prog. Phys.* **81**, 056503 (2018).
- [4] N. H. Bonadeo, J. Erland, D. Gammon, D. Park, D. S. Katzer, and D. G. Steel, Coherent optical control of the quantum state of a single quantum dot, *Science* **282**, 1473 (1998).
- [5] W. F. Koehl, B. B. Buckley, F. J. Heremans, G. Calusine, and D. D. Awschalom, Room temperature coherent control of defect spin qubits in silicon carbide, *Nature (London)* **479**, 84 (2011).
- [6] T. Faust, J. Rieger, M. J. Seitner, J. P. Kotthaus, and E. M. Weig, Coherent control of a classical nanomechanical two-level system, *Nat. Phys.* **9**, 485 (2013).
- [7] A. V. Kimel, A. Kirilyuk, F. Hansteen, R. V. Pisarev, and T. Rasing, Nonthermal optical control of magnetism and ultrafast laser-induced spin dynamics in solids, *J. Phys.: Condens. Matter* **19**, 043201 (2007).
- [8] E. Rozkotova, P. Nemeč, N. Tesarova, P. Maly, V. Novak, K. Olejnik, M. Cukr, and T. Jungwirth, Coherent control of magnetization precession in ferromagnetic semiconductor (Ga, Mn)As, *Appl. Phys. Lett.* **93**, 232505 (2008).
- [9] A. P. Heberle, J. J. Baumberg, and K. Köhler, Ultrafast coherent control and destruction of excitons in quantum wells, *Phys. Rev. Lett.* **75**, 2598 (1995).
- [10] A. M. Weiner, J. P. Heritage, and E. M. Kirschner, High-resolution femtosecond pulse shaping, *J. Opt. Soc. Am. B* **5**, 1563 (1988).
- [11] T. Wolz, A. Stehli, A. Schneider, I. Boverter, R. Macêdo, A. V. Ustinov, M. Kläui, and M. Weides, Introducing coherent time control to cavity magnon-polariton modes, *Commun. Phys.* **3**, 3 (2020).
- [12] M. F. Limonov, M. V. Rybin, A. N. Poddubny, and Y. S. Kivshar, Fano resonances in photonics, *Nat. Photon.* **11**, 543 (2017).
- [13] A. G. Gurevich and G. A. Melkov, *Magnetization Oscillations and Waves* (Taylor & Francis, London, 1996).
- [14] J. Atulasimha and A. B. A. Flatau, A review of magnetostrictive iron-gallium alloys, *Smart Mater. Struct.* **20**, 043001 (2011).
- [15] C.-M. Park, J. A. Bain, T. W. Clinton, P. A. A. van der Heijden, and T. J. Klemmer, Measurement of Ga implantation profiles in the sidewall and bottom of focused-ion-beam-etched structures, *Appl. Phys. Lett.* **84**, 3331 (2004).
- [16] J. B. Restorff, M. Wun-Fogle, K. B. Hathaway, A. E. Clark, T. A. Lograsso, and G. Petculescu, Tetragonal magnetostriction and magnetoelastic coupling in Fe-Al, Fe-Ga, Fe-Ge, Fe-Si, Fe-Ga-Al, and Fe-Ga-Ge alloys, *J. Appl. Phys.* **111**, 023905 (2012).
- [17] A. E. Clark, M. Wun-Fogle, J. B. Restorff, K. W. Dennis, T. A. Lograsso, and R. W. McCallum, Temperature dependence of the magnetic anisotropy and magnetostriction of Fe_{100-x}Ga_x ($x = 8.6, 16.6, 28.5$), *J. Appl. Phys.* **97**, 10M316 (2005).
- [18] D. Nardi, M. Travaglini, M. E. Siemens, Q. Li, M. M. Murnane, H. C. Kapteyn, G. Ferrini, F. Parmigiani, and F. Banfi, Probing thermomechanics at the nanoscale: Impulsively excited pseudo-surface acoustic waves in hypersonic phononic crystals, *Nano Lett.* **11**, 4126 (2011).
- [19] B. Obyr, T. Meyer, P. Pirro, T. Brächer, B. Lägél, J. Osten, T. Strache, J. Fassbender, and B. Hillebrands, Microscopic magnetic structuring of a spin-wave waveguide by ion implantation in a Ni₈₁Fe₁₉, *Appl. Phys. Lett.* **102**, 022409 (2013).
- [20] S. M. Kukhtaruk, A. W. Rushforth, F. Godejohann, A. V. Scherbakov, and M. Bayer, Transition magnon modes in thin ferromagnetic nanogratings, *Phys. Rev. B* **106**, 064411 (2022).
- [21] See Supplemental Material at <http://link.aps.org/supplemental/10.1103/PhysRevResearch.6.L012019> for the magnon and phonon mode profiles, the parameters of numerical solution of the Landau-Lifshitz-Gilbert equation, derivation of the analytical solution, and the power dependence of the magnon spectra. For the calculations, we used the material parameters from Refs. [16,17,64–67].
- [22] C. Thomsen, H. T. Grahn, H. J. Maris, and J. Tauc, Surface generation and detection of phonons by picosecond light pulse, *Phys. Rev. B* **34**, 4129 (1986).
- [23] M. van Kampen, C. Jozsa, J. T. Kohlhepp, P. LeClair, L. Lagae, W. J. M. de Jonge, and B. Koopmans, All-optical probe of coherent spin waves, *Phys. Rev. Lett.* **88**, 227201 (2002).
- [24] W. K. Hiebert, A. Stankiewicz, and M. R. Freeman, Direct observation of magnetic relaxation in a small permalloy disk by time-resolved scanning Kerr microscopy, *Phys. Rev. Lett.* **79**, 1134 (1997).
- [25] A. Bartels, R. Cerna, C. Kistner, A. Thoma, F. Hudert, C. Janke, and T. Dekorsy, Ultrafast time-domain spectroscopy based on high-speed asynchronous optical sampling, *Rev. Sci. Instrum.* **78**, 035107 (2007).
- [26] C. Thomsen, H. T. Grahn, H. J. Maris, and J. Tauc, Picosecond interferometric technique for study of phonons in the Brillouin frequency range, *Opt. Commun.* **60**, 55 (1986).

- [27] L. Dreher, M. Weiler, M. Pernpeintner, H. Huebl, R. Gross, M. S. Brandt, and S. T. B. Goennenwein, Surface acoustic wave driven ferromagnetic resonance in nickel thin films: Theory and experiment, *Phys. Rev. B* **86**, 134415 (2012).
- [28] H. Y. Yuan, Y. Cao, A. Kamra, R. A. Duine, and P. Yan, Quantum magnonics: When magnon spintronics meets quantum information science, *Phys. Rep.* **965**, 1 (2022).
- [29] B. Z. Rameshti, S. V. Kusminskiy, J. A. Haigh, K. Usami, D. Lachance-Quirion, Y. Nakamura, C.-M. Hu, H. X. Tang, G. E. W. Bauer, and Y. M. Blanter, Cavity magnonics, *Phys. Rep.* **979**, 1 (2022).
- [30] H.-P. Breuer and F. Petruccione, *The Theory of Open Quantum Systems* (Oxford University Press, Oxford, 2006).
- [31] N. K. P. Babu, A. Trzaskowska, P. Graczyk, G. Centała, S. Mieszczak, H. Głowiński, M. Zdunek, S. Mielcarek, and J. W. Klos, The interaction between surface acoustic waves and spin waves: The role of anisotropy and spatial profiles of the modes, *Nano Lett.* **21**, 946 (2021).
- [32] G. Malinowski, F. Dalla Longa, J. H. H. Rietjens, P. V. Paluskar, R. Huijink, H. J. M. Swagten, and B. Koopmans, Control of speed and efficiency of ultrafast demagnetization by direct transfer of spin angular momentum, *Nat. Phys.* **4**, 855 (2008).
- [33] D. Rudolf, C. La-O-Vorakiat, M. Battiato, R. Adam, J. M. Shaw, E. Turgut, P. Maldonado, S. Mathias, P. Grychtol, H. T. Nembach, T. J. Silva, M. Aeschlimann, H. C. Kapteyn, M. M. Murnane, C. M. Schneider, and P. M. Oppeneer, Ultrafast magnetization enhancement in metallic multilayers driven by superdiffusive spin current, *Nat. Commun.* **3**, 1037 (2012).
- [34] G.-M. Choi, B.-C. Min, K.-J. Lee, and D. G. Cahill, Spin current generated by thermally driven ultrafast demagnetization, *Nat. Commun.* **5**, 4334 (2014).
- [35] A. J. Schellekens, K. C. Kuiper, R. R. J. C. de Wit, and B. Koopmans, Ultrafast spin-transfer torque driven by femtosecond pulsed-laser excitation, *Nat. Commun.* **5**, 4333 (2014).
- [36] I. Razdolski, A. Alekhin, N. Ilin, J. P. Meyburg, V. Roddatis, D. Diesing, U. Bovensiepen, and A. Melnikov, Nanoscale interface confinement of ultrafast spin transfer torque driving non-uniform spin dynamics, *Nat. Commun.* **8**, 15007 (2017).
- [37] Q. Remy, J. Hohlfeld, M. Vergès, Y. Le Guen, J. Gorchon, G. Malinowski, S. Mangin, and M. Hehn, Accelerating ultrafast magnetization reversal by non-local spin transfer, *Nat. Commun.* **14**, 445 (2023).
- [38] J. Igarashi, W. Zhang, Q. Remy, E. Diaz, J.-X. Lin, J. Hohlfeld, M. Hehn, S. Mangin, J. Gorchon, and G. Malinowski, Optically induced ultrafast magnetization switching in ferromagnetic spin valves, *Nat. Mater.* **22**, 725 (2023).
- [39] C. Abert, H. Sepelri-Amin, F. Bruckner, C. Vogler, M. Hayashi, and D. Suess, Fieldlike and dampinglike spin-transfer torque in magnetic multilayers, *Phys. Rev. Appl.* **7**, 054007 (2017).
- [40] T. L. Linnik, A. V. Scherbakov, D. R. Yakovlev, X. Liu, J. K. Furdyna, and M. Bayer, Theory of magnetization precession induced by a picosecond strain pulse in ferromagnetic semiconductor (Ga, Mn)As, *Phys. Rev. B* **84**, 214432 (2011).
- [41] N. Kazantseva, U. Nowak, R. W. Chantrell, J. Hohlfeld, and A. Rebei, Slow recovery of the magnetisation, *Europhys. Lett.* **81**, 27004 (2008).
- [42] D. E. Parkes, L. R. Sheldford, P. Wadley, V. Holý, M. Wang, A. T. Hindmarch, G. van der Laan, R. P. Champion, K. W. Edmonds, S. A. Cavill, and A. W. Rushforth, Magnetostrictive thin films for microwave spintronics, *Sci. Rep.* **3**, 2220 (2013).
- [43] A. V. Scherbakov, A. P. Danilov, F. Godejohann, T. L. Linnik, B. A. Glavin, L. A. Shelukhin, D. P. Pattnaik, M. Wang, A. W. Rushforth, D. R. Yakovlev, A. V. Akimov, and M. Bayer, Optical excitation of single- and multi-mode magnetization precession in galfenol, *Phys. Rev. Appl.* **11**, 031003(R) (2019).
- [44] J. Janušonis, C. L. Chang, P. H. M. van Loosdrecht, and R. I. Tobey, Frequency tunable surface magneto-elastic waves, *Appl. Phys. Lett.* **106**, 181601 (2015).
- [45] J. V. Jäger, A. V. Scherbakov, B. A. Glavin, A. S. Salasyuk, R. P. Champion, A. W. Rushforth, D. R. Yakovlev, A. V. Akimov, and M. Bayer, Resonant driving of magnetization precession in a ferromagnetic layer by coherent monochromatic phonons, *Phys. Rev. B* **92**, 020404(R) (2015).
- [46] M. Deb, E. Popova, M. Hehn, N. Keller, S. Mangin, and G. Malinowski, Picosecond acoustic-excitation-driven ultrafast magnetization dynamics in dielectric Bi-substituted yttrium iron garnet, *Phys. Rev. B* **98**, 174407 (2018).
- [47] Y. Hashimoto, D. Bossini, T. H. Johansen, E. Saitoh, A. Kirilyuk, and T. Rasing, Frequency and wavenumber selective excitation of spin waves through coherent energy transfer from elastic waves, *Phys. Rev. B* **97**, 140404(R) (2018).
- [48] A. S. Salasyuk, A. V. Rudkovskaya, A. P. Danilov, B. A. Glavin, S. M. Kukhtaruk, M. Wang, A. W. Rushforth, P. A. Nekludova, S. V. Sokolov, A. A. Elistratov, D. R. Yakovlev, M. Bayer, A. V. Akimov, and A. V. Scherbakov, Generation of localized microwave magnetic field by coherent phonons in a ferromagnetic nanograting, *Phys. Rev. B* **97**, 060404(R) (2018).
- [49] C. Berk, M. Jaris, W. Yang, S. Dhuey, S. Cabrini, and H. Schmidt, Strongly coupled magnon-phonon dynamics in a single nanomagnet, *Nat. Commun.* **10**, 2652 (2019).
- [50] H. Liu, M. T. Trinh, E. M. Clements, D. Sapkota, L. Li, Z. Romestan, S. Bhat, V. Mapara, A. Barua, S. L. Carrera, M.-H. Phan, D. Arena, H. Srikanth, D. Mandrus, A. H. Romero, and D. Karaiskaj, Elastically induced magnetization at ultrafast time scales in a chiral helimagnet, *Phys. Rev. B* **106**, 035103 (2022).
- [51] X. Yang, M. Yu, D.-L. Kwong, and C. W. Wong, All-optical analog to electromagnetically induced transparency in multiple coupled photonic crystal cavities, *Phys. Rev. Lett.* **102**, 173902 (2009).
- [52] N. Pramanik, K. C. Yellapragada, S. Singh, and P. A. Lakshmi, Coherent control of Fano resonances in a macroscopic four-mirror cavity, *Phys. Rev. A* **101**, 043802 (2020).
- [53] G. D. Fuchs, V. V. Dobrovitski, D. M. Toyli, F. J. Heremans, C. D. Weis, T. Schenkel, and D. D. Awschalom, Excited-state spin coherence of a single nitrogen-vacancy centre in diamond, *Nat. Phys.* **6**, 668 (2010).
- [54] E. R. MacQuarrie, T. A. Gosavi, N. R. Jungwirth, S. A. Bhawe, and G. D. Fuchs, Mechanical spin control of nitrogen-vacancy centers in diamond, *Phys. Rev. Lett.* **111**, 227602 (2013).
- [55] V. V. Belykh, A. R. Korotneva, and D. R. Yakovlev, Stimulated resonant spin amplification reveals millisecond electron spin coherence time of rare-earth ions in solids, *Phys. Rev. Lett.* **127**, 157401 (2021).
- [56] X. Zhang, C.-L. Zou, L. Jiang, and H. X. Tang, Cavity magnomechanics, *Sci. Adv.* **2**, e1501286 (2016).
- [57] X. Zhang, C.-L. Zou, L. Jiang, and H. X. Tang, Strongly coupled magnons and cavity microwave photons, *Phys. Rev. Lett.* **113**, 156401 (2014).

- [58] N. Crescini, C. Braggio, G. Carugo, R. Di Vora, A. Ortolan, and G. Ruoso, Magnon-driven dynamics of a hybrid system excited with ultrafast optical pulses, *Commun. Phys.* **3**, 164 (2020).
- [59] R. Cheng, D. Xiao, and A. Brataas, Terahertz antiferromagnetic spin Hall nano-oscillator, *Phys. Rev. Lett.* **116**, 207603 (2016).
- [60] J. R. Hortensius, D. Afanasiev, M. Matthiesen, R. Leenders, R. Citro, A. V. Kimel, R. V. Mikhaylovskiy, B. A. Ivanov, and A. D. Caviglia, Coherent spin-wave transport in an antiferromagnet, *Nat. Phys.* **17**, 1001 (2021).
- [61] P. Peng, Y. Mi, M. Lytova, M. Britton, X. Ding, A. Yu. Naumov, P. B. Corkum, and D. M. Villeneuve, Coherent control of ultrafast extreme ultraviolet transient absorption, *Nat. Photon.* **16**, 45 (2022).
- [62] M. F. Limonov, Fano resonance for application, *Adv. Opt. Photon.* **13**, 703 (2021).
- [63] M. Fleischhauer, A. Imamoglu, and J. P. Marangos, Electromagnetically induced transparency: Optics in coherent media, *Rev. Mod. Phys.* **77**, 633 (2005).
- [64] D. E. Parkes, S. A. Cavill, A. T. Hindmarch, P. Wadley, F. McGee, C. R. Staddon, K. W. Edmonds, R. P. Campion, B. L. Gallagher, and A. W. Rushforth, Non-volatile voltage control of magnetization and magnetic domain walls in magnetostrictive epitaxial thin films, *Appl. Phys. Lett.* **101**, 072402 (2012).
- [65] A. E. Clark, K. B. Hathaway, M. Wun-Fogle, J. B. Restorff, T. A. Lograsso, V. M. Keppens, G. Petculescu, and R. A. Taylor, Extraordinary magnetoelasticity and lattice softening in bcc Fe-Ga alloys, *J. Appl. Phys.* **93**, 8621 (2003).
- [66] H. Ulrichs and I. Razdolski, Micromagnetic view on ultrafast magnon generation by femtosecond spin current pulses, *Phys. Rev. B* **98**, 054429 (2018).
- [67] O. Madelung, *Semiconductors: Data Handbook* (Springer, Berlin, 2004).